can take any value from zero to infinity, and an independent experimental determination of this parameter x, i.e., the gap parameter $\Delta(\Gamma_s, 0)$, is desirable to verify the present theory.

[13]See, for example, Schrieffer (Ref. 6), p. 162; A. B. Migdal, Zh. Eksperim. i Teor. Fiz. 34, 1438 (1958)[Sov. Phys. JETP 7, 996 (1958)].

[14]L. H. Palmer and M. Tinkham, Phys. Rev. 165, 588 (1968); W. Shaw and J. C. Swihart, Phys. Rev. Letters 20, 1000 (1968); T. A. Fulton and D. E. McCumber, Phys. Rev. 175, 585 (1968); S. B. Nam (unpublished).

[15]A. A. Abrikosov, Zh. Eksperim. i Teor. Fiz. 32, 1442 (1957) [Sov. Phys. JETP 5, 1174 (1957)].

[16]V. L. Ginzburg and L. D. Landau, Zh. Eksperim. i Teor. Fiz. 20, 1064 (1950).

[17]W. H. Kleiner, L. M. Roth, and S. H. Autler, Phys. Rev. 133, A1226 (1964).

[18]The equivalent result has been obtained by several authors: A. I. Larkin, Zh. Eksperim. i Teor. Fiz. 48, 232 (1965)[Sov. Phys. JETP 21, 153 (1965)]; P. Fulde and K. Maki, Phys. Rev. 139, A788 (1965); K. Maki, *ibid.* 148, 362 (1966).

[19]S. B. Nam, J. Korean Phys. Soc. (to be published).

[20]J. Bardeen and M. J. Stephen, Phys. Rev. 140, A1197 (1965).

PHYSICAL REVIEW B VOLUME 3, NUMBER 9 1 MAY 1971

Phonon Generation and Detection in Superconducting Lead Diodes

A. H. Dayem, B. I. Miller, and J. J. Wiegand
Bell Telephone Laboratories, Holmdel, New Jersey 07733

(Received 30 November 1970)

We present a detailed experimental study of the behavior of Pb-Pb superconducting diodes in phonon generation and detection. It is shown that the detection process occurs via pair breaking as well as phonon-assisted tunneling. The present experimental results do not resolve the distribution in energy of the phonons emitted by the generator. However, the derivative of the detected signal with respect to the generator current contains well-defined structure coincident with the phonon density of states of Pb calculated by McMillan and Rowell.

I. INTRODUCTION

Superconducting tunnel diodes have been successfully used[1] as phonon generators and detectors. Since then we set as our goal the experimental determination of at least the coarse features of the generated phonon spectrum for various levels of excitation and an understanding of the mechanisms responsible for the detection process. This information is essential if such a device is to be used for studying propagation and absorption of phonons in solids or in liquid helium in a frequency range not attainable by conventional ultrasonic devices.

We use superconductor-barrier-superconductor tunnel diodes evaporated on two parallel faces of a sapphire single crystal ~1 cm long and 1 cm diameter. The diode area is 0.1×0.1 cm and the film thickness is $\sim 1.5\times10^{-5}$ cm. To the diode used as phonon generator, we apply pulses of amplitude $V > 2\Delta$, where 2Δ is the energy gap of the superconductor and V is in electron volts. The excited quasiparticles produced by tunneling relax and recombine emitting phonons.[2,3] The relaxation produces phonons of energy ω in the range $0<\omega<V-2\Delta$ while the recombination into Cooper pairs produces phonons of $\omega \gtrsim 2\Delta$. Some of the generated phonons propagate in the sapphire crystal in rectilinear trajectories to the detecting diode. Coincident with the time of arrival of the phonons, a voltage pulse S is measured across the detector which is biased at a voltage $V_B < 2\Delta$ from a dc constant-current source. The major contribution to the signal S comes from those incident phonons of $\omega \geq 2\Delta$.[1] Such phonons break Cooper pairs in the detector resulting in an increase in the quasiparticle population above the gap edge, and hence an enhancement in the tunneling current at $V_B < 2\Delta$. Using this simple model for phonon generation and detection, an adequate interpretation was obtained for previously published results.[1] In the following paragraphs we discuss some details of the electron-phonon and electron-electron interactions relevant to phonon generation in superconducting tunnel diodes.

First we discuss the decay thresholds and their effects on the generated phonon spectrum. Excited particles of energy $E \sim \Delta$ will either directly recombine in pairs emitting phonons of energy $\omega \geq 2\Delta$ or first individually decay to the top of the gap emitting relaxation phonons with $\omega = E - \Delta$ and then recombine in pairs emitting phonons with $\omega = 2\Delta$. Since at $E = \Delta$ the group velocity of an excited quasiparticle is zero, the threshold[2,3] E_d for the relaxation process is given by $(E_d - \Delta) \geq 8 v_s^2 v_F^{-2} \Delta$ where v_s is the sound velocity and v_F is the electron velocity at the Fermi level. This threshold is of the order of $2\times10^{-5}\Delta$ for the longitudinal and $0.26\times10^{-5}\Delta$ for the transverse phonons in Pb. Ignoring gap anisotropy, the recombination phonons are emitted in an extremely

narrow band of width $\delta\omega$, where $\delta\omega/2\Delta$ is of the order 10^{-5} for the longitudinal and 10^{-6} for the transverse phonon modes, and hence the phonon spectrum emitted from a superconducting tunnel diode contains an essentially monochromatic peak at $\omega = 2\Delta$. However, the width $\delta\omega$ is determined by the probability that a quasiparticle of energy $\sim E_d$ would first relax to the top of the gap emitting a phonon of energy $\omega_d = E_d - \Delta$. This probability is proportional to the phonon density of states at ω_d. This density is extremely small as evident in the Pb phonon spectrum calculated by McMillan and Rowell.[4] Furthermore, phonons of energy ω_d have a wavelength 2 to 3 orders of magnitude larger than the film thickness. Therefore, such phonons can only be emitted with wave vectors in the plane of the film, resulting in a reduction in the emission probability.[5] Since, in addition the electron interaction with long-wavelength phonons is heavily screened by the dielectric constant of the metal, one expects that direct recombination will extend far beyond the threshold E_d and may lend itself to a direct experimental determination.

Our scheme to measure the direct recombination width in Pb is to use a detector made out of Pb-Bi alloy (both stripes) with a gap slightly larger than Pb. By careful measurements using detectors with progressively larger gaps we hope not only to determine the threshold but also the "line shape" as determined by the ratio of excitations directly recombining to those relaxing first to the top of the gap.

The other threshold of interest is that occurring at $E = 3\Delta$. Here a particle with $E \geq 3\Delta$ would either relax to the top of the gap emitting a phonon with $\omega \geq 2\Delta$ or break a Cooper pair, resulting in three excited particles of energies E_1, E_2, and E_3 such that $E = E_1 + E_2 + E_3$. It is obvious, however, that these two processes are indistinguishable in our type of experiment if both generator and detector are made out of the same superconductor since the final number of phonons emitted with $\omega \geq 2\Delta$ is the same in both cases. But in an experiment where the detector gap is larger than the generator gap as described in the previous paragraph one is capable of detecting which process is predominant. This can be explained as follows: Consider for the moment that a number of excitations is produced with $E = 4\Delta$. If pair breaking is the dominant process, one would obtain, say, $E_1 = E_2 = \Delta$ and $E_3 = 2\Delta$, the latter giving a relaxation phonon of $\omega = \Delta$. However, if the excitations relax directly to the top of the gap, a number of phonons of energy $\omega = 3\Delta$ is produced. In spite of the possibility of phonon reabsorption[6] some of the 3Δ phonons will escape into the sapphire. Only in this latter case will the larger gap detector show an enhancement of the signal by an amount proportional to the number of 3Δ phonons that escaped.

For higher excitation energies, and in particular when $\omega = E - \Delta$ lies in the vicinity of one of the phonon peaks $\omega_t = 4.45$ meV and $\omega_l = 8.5$ meV we encounter new difficulties. As discussed by Scalapino[7] the lifetime of such quasiparticles is so short that their level width is comparable with their excitation energy. The concept of a quasiparticle occupying a well-defined level E breaks down and the statement that it will relax to the top of the gap emitting a phonon of $\omega = E - \Delta$ becomes meaningless. Indeed, a total excitation energy E has been added to the system and its final decay to the top of the gap will increase the energy of the phonon gas by $(E - \Delta)$ which is in general distributed among various phonon modes including those around $\omega = E - \Delta$.

In the experiment, we use diodes whose resistance is typically of the order 10^{-2} to 10^{-3} Ω and the generator is driven by a current of several amperes. Assuming the lifetime of an excitation to be 10^{-10}–10^{-13} sec the steady state in the generator will contain some 10^{16}–10^{13} excited particles/cm^3 and a large population of phonons. The spectrum of the phonons escaping into the substrate could be calculated from the detailed balance at each energy level between the electrons and the phonons using interaction rates appropriate to the degree of excitation of the system. The interactions to be taken into account are the Coulomb interaction given by the pseudopotential μ^* and the electron-phonon interaction described by the function $\alpha^2(\omega)F(\omega)$, where α^2 is the effective electron-phonon coupling, F is the phonon density of states, and ω is the phonon energy. Both μ^* and α^2F have been calculated for a number of superconductors by McMillan and Rowell.[4] In addition, one should also consider the possible interactions among the large number of excitations present in the generator. The calculation of the emitted phonon spectrum is quite complicated and we will concentrate here on presenting the experimental results in full detail and compare them with crude calculations based on the simplest possible models.

In this paper we present experimental results showing the behavior of Pb diodes both as phonon generators and detectors. The experimental techniques are described in Sec. II. In Sec. III, simplified models of the generator and detector are described and their behavior is calculated in the range where first-order relaxation processes are valid. This is followed by a presentation of the experimental results and a comparison between theoretical and actual behavior in Sec. V.

II. EXPERIMENTAL TECHNIQUES

The samples were evaporated on two parallel faces of a sapphire single crystal as shown schematically in Fig. 1. The sample holder was de-

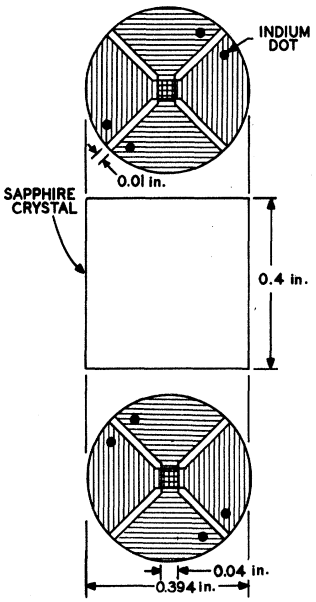

FIG. 1. Schematic drawing showing the configuration of the evaporated samples to minimize inductive coupling between generator and detector.

signed to provide for each pair of indium dots a pair of pressure contacts connected to a floating low-impedance coaxial line. Each line and its pressure contacts is individually enclosed in a continuous ground shield. This together with the particular geometry and arrangement of the In dots shown in Fig. 1 reduced to a negligible amount the inductive coupling between input and output of one diode as well as that between generator and detector. To the generator we apply dc pulses 3–4 μsec wide at a repetition rate 1000 Hz. The generator pulse current I and voltage V are fed to a dual trace sampling scope. A dc bias $V_B < 2\Delta$ is applied to the detector and its pulse output S is amplified and fed into a second sampling scope. The sampling points are positioned ~ 2 μsec beyond the leading edges of the generator and signal pulses, respectively, thus taking the acoustic time of flight into account. The outputs from the sampling scopes are fed either to x-y recorders or to a data-acquisition system (to be referred to as DAS for short) which transfers the input in digital form to a magnetic tape. Our DAS has three digital voltmeters which permit us to record three separate channels simultaneously. There are also 24 additional channels which can be recorded sequentially.

To obtain the derivatives $\partial V/\partial I$ and $\partial S/\partial I$ we developed the following scheme. We use a function generator running at 500 cps with two outputs; one supplies a square wave, the other a sine wave. Part of the square-wave output is used to trigger the modulation pulse generator at 500 cps. The other part is differentiated, full wave rectified, and amplified to trigger the main pulse generator at 1000 cps. The sine-wave output from the function generator is used to drive the reference channels of two lock-in amplifiers. The modulation pulser is connected through an isolation network in parallel with the main pulser and the two pulse trains are aligned in position and width. The isolation network is necessary to ensure the constancy of the modulation pulse height at all values of the main pulse. Since the diode resistance is always extremely small, all sources, pulsed and dc, operate in a constant-current mode as seen at the diode terminals. When the modulation pulse is applied, the output from the sampling scopes contains a square-wave component at 500 cps. The V and S outputs are then fed through a bandpass filter or directly into the signal channel of the lock-in amplifiers and provide a dc output proportional to $\partial V/\partial I$ and $\partial S/\partial I$.

The data are recorded on magnetic tape in the form of separate files or sets containing either (V, I, S) or $(V, \partial V/\partial I, \partial S/\partial I)$ or (V_B, I_B, S), where V_B and I_B are the detector bias voltage and current, respectively. Each data set contains about 1000 points. To drive the various components of the experimental setup we use a timer, a stepper motor, and high-resolution potentiometers. The timer pulse energizes the stepper motor power supply. After the step is completed a command pulse is produced and fed into the DAS which records simultaneously the three channels of interest. The cycle is then repeated every 3 or 12.6 sec when the integration time of the digital voltmeters is 1 or 10 sec, respectively.

Using IBM System/360 the binary-coded decimal data on tape are read and stored permanently on a private disc pack. To simplify subsequent programming and analysis the raw experimental sets are converted such that the independent variable V or V_B is equally spaced. We use linear interpolation to compute about 500 equally spaced points. This procedure introduces only a negligible amount of smoothing and the equally spaced set still contains all the noise and information in the raw set.

This completes the description of the experimental techniques. Before proceeding to Sec. III we would like, however, to discuss some aspects of the detector characteristic which are relevant to the present study. As mentioned previously, the detector is biased at $V_B < 2\Delta$. In this region the current is composed of a complicated superposition of contributions coming from various sources.[8] All contributions are more or less of the same order of magnitude. The I-V characteristic and probably also the way the various contributions add up are highly nonlinear. We summarize some of these contributions and their possible effect on our measurements. The order of magnitude quoted for each

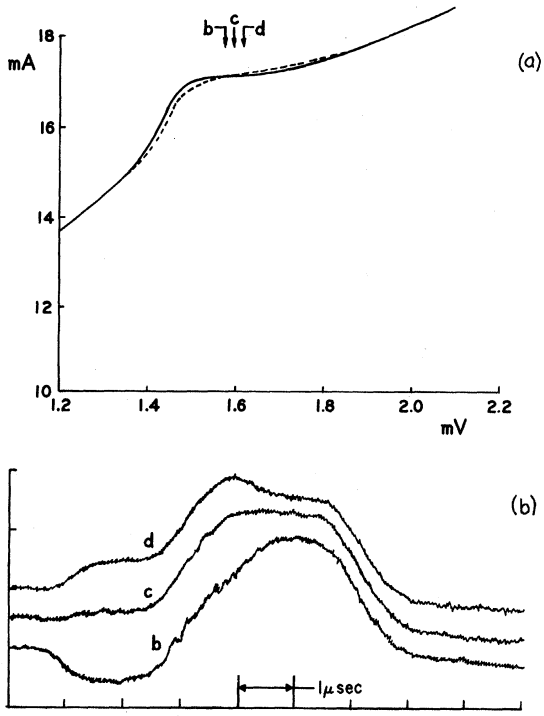

FIG. 2. Effect of the dc magnetic field associating with the generator current on the detected signal pulse. (a) The I_B - V_B characteristic showing the resonance peak and its rotation (dashed line) with increasing magnetic field. The detector pulse shapes labeled by *b*, *c*, and *d* in (b) correspond to detector bias indicated in (a) by the arrows labeled by *b*, *c*, and *d*, respectively.

contribution is estimated relative to the current flowing at the same voltage when the films are normal.

(a) The tunneling current due to thermally excited quasiparticles should be of the order 10^{-7} in Pb diodes at 1 °K.

(b) Leakage current[9] of unknown origin appears to be linearly dependent on the voltage and is of the order $1-3\times10^{-2}$ in our samples. It may contribute phonons having a Planck's distribution (heat).

(c) Structure due to the self-detection of the ac Josephson current appears in one of two forms: the well-known Fiske constant voltage steps[10] at the resonance frequencies of the strip-line modes which are well defined and numerous for $V<\Delta$, and the resonance peak[10] which occurs at voltages where the separation between modes and their respective Q's are so small that their separate structure is washed out. This structure is extremely sensitive to magnetic fields and is sufficiently strong to dominate the characteristic in a perfect diode producing currents of order 10^{-2}. Obviously, the voltage region where the resonance steps occur was excluded from our measurements. However, by properly adjusting the magnetic field it was possible to move the resonance peak to a position on the characteristic such that a region of relatively high dynamic resistance, and hence an enhancement of the signal, was obtained. Operation with a fixed bias at the peak, though desirable, proved to be quite tedious. Small drifts in the bias voltage result in large changes in the signal. More serious, however, is the effect of the magnetic field associating with the generator pulse current. This magnetic field acts essentially as a dc field adding to or subtracting from the externally applied field resulting in a rotation of the characteristic about a point adjacent to the position of the peak as shown in Fig. 2(a). This drastically modifies the shape of the received signal pulse as shown in Fig. 2(b). We emphasize that this is a "dc" effect and as seen in Fig. 2(b) the ac inductive coupling is barely discernible. Operation in this mode was usually avoided where possible by increasing the magnetic field sufficiently till the resonance peak disappears and the I-V characteristic becomes stationary with moderately large changes of the magnetic field.

(d) Finally there is the so-called subharmonic structure occurring at $V_B = 2\Delta/n$ where n is an integer. This structure, though not well understood, has been the subject of a recent study by Giaever and Zeller[8] who attributed it to the self-detection of the Josephson radiation.[8] Our results show some peculiarities associated with this structure and may contribute to a better understanding of its nature.

III. THEORY

In the experiment the applied pulses are sufficiently wide (3–4 μsec) that a steady state is established in both generator and detector. The phonon pulse incident on the detector will produce an increment $i(V_B)$ in the current where $V_B < 2\Delta$ is the bias voltage. Since $i(V_B)$ will have the duration of the phonon pulse the transient response of the detector can be calculated using the simple equivalent circuit of Fig. 3. Here I_B is supplied to the diode from a constant-current source and the arrival of the phonon pulse is simulated by closing the switch at time $t=0$ reducing the diode resistance at the bias point from R_B to R_B'. The voltage appearing across the load resistance R_L is given by

$$S(t) = -I_B(R_B - R_B')(R_B' + R_L)^{-1} R_L e^{-t/t_0},$$

with

$$t_0 = C(R_B' + R_L).$$

The diode time constant $R_B C_B$ is small compared to t_0 and was ignored. If $i \ll I_B$, one may linearize the characteristic and put $I_B(R_B - R_B') = iR_d$ where R_d is the dynamic resistance at the bias point. With $t_0 \gg$ pulse duration, the signal-pulse amplitude is then

$$S = iR_d(1 + R_B/R_L)^{-1}. \quad (1)$$

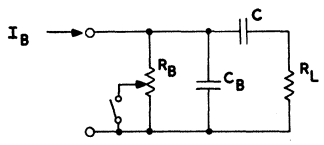

FIG. 3. Simplified equivalent circuit of the detector.

Our experimental results show that probably three different mechanisms are contributing to $i(V_B)$. The largest contribution comes from the pair-breaking mechanism[1,6] (PBM for short), described in the Introduction. The second comes from phonon-assisted tunneling[11] (PAT) while the third is from an unknown source and produces well-defined steps at the "subharmonic" voltages $2\Delta/n$. These mechanisms will be discussed later in more detail and we proceed here to calculate the current $i(V_B)$ coming from PBM. We assume that incident phonons with $\omega \geq 2\Delta$ produce a steady-state population n_e of excitations which occupy the states in the energy range $\Delta \leq E \leq \Delta + \delta$ on either side of the barrier of an ideal diode at absolute zero. At a bias V_B the current will be given by the usual tunneling expression

$$i(V_B) = \frac{1}{R} \int_{V_B+\Delta}^{V_B+\Delta+\delta} \frac{E(E-V_B)dE}{\left\{(E^2-\Delta^2)[(E-V_B)^2-\Delta^2]\right\}^{1/2}},$$

where R is the normal-state resistance. Since $\delta \ll \Delta$ one can take the density of empty states as a constant equal to its value at $V_B + \Delta$ and obtain

$$i(V_B) = \frac{1}{R} \frac{V_B+\Delta}{[(V_B+\Delta)^2-\Delta^2]^{1/2}} \int_{V_B+\delta}^{V_B+\Delta+\delta} \frac{(E-V_B)dE}{[(E-V_B)^2-\Delta^2]^{1/2}}$$

$$\cong \frac{2\Delta}{R} \left(\frac{\delta}{2\Delta}\right)^{1/2} \frac{V_B+D}{[(V_B+D)^2-\Delta^2]^{1/2}}, \qquad (2)$$

where $(\delta/2\Delta)^{1/2}$ is related to n_e by the expression

$$(\delta/2\Delta)^{1/2} = n_e/4\Delta N(0)Ad, \qquad (3)$$

where $N(0)$ is the density of states for one spin at the Fermi level, while A is the area, and d is the total (both films) thickness of the diode. To relate n_e to the phonon density in the incident shower we must use the detailed balance equations.[12]

We derive equations to describe the detailed balance in a simple three-level system which is appropriate for the generator with $V \leq 6\Delta$ as well as for the detector. Although in the steady state the results obtained for the generator are obvious, the equations may be useful in applications where the applied pulses are too narrow to establish the steady state; they also provide in a concise fashion the manner in which one should calculate the number of phonons of $\omega \geq 2\Delta$ for $V > 4\Delta$.

In the generator the tunneling current I produces identical excitations on either side of the barrier. These excitations are distributed in energy as shown in Fig. 4(a) and the number produced per second in the energy range between E and $E+dE$ is proportional to

$$f(E, V)\,dE = \frac{E(V-E)\,dE}{\left\{(E^2-\Delta^2)[(V-E)^2-\Delta^2]\right\}^{1/2}}, \qquad (4)$$

where the current is

$$I = \frac{1}{R} \int_{\Delta}^{V-\Delta} f(E, V)\,dE. \qquad (5)$$

Concentrating on phonons of $\omega \geq 2\Delta$ the current I is divided into two parts

$$I_1 = \frac{1}{R} \int_{\Delta}^{3\Delta} f(E, V)\,dE \qquad (6)$$

and

$$I_2 = \frac{1}{R} \int_{3\Delta}^{V-\Delta} f(E, V)\,dE. \qquad (7)$$

If we ignore all processes which involve phonons of $\omega < 2\Delta$ the generator may be represented by the three-level system shown in Fig. 4(b). It consists of 3 electron levels: a Fermi level 0 containing all condensed pairs and two excited levels 1 and 2 at energies Δ and 3Δ, respectively. The electrons are interacting with a bath of phonons of $\omega = 2\Delta$ and of total population N_p. The whole system is in contact with a medium at constant temperature. The permissible transitions are (i) single-particle transition from 1 to 2 (2 to 1) absorbing (emitting) a phonon of $\omega = 2\Delta$; (ii) pair condensation (breaking) from 1 to 0 (0 to 1) emitting (absorbing) a phonon of $\omega = 2\Delta$; (iii) no transitions are permissible be-

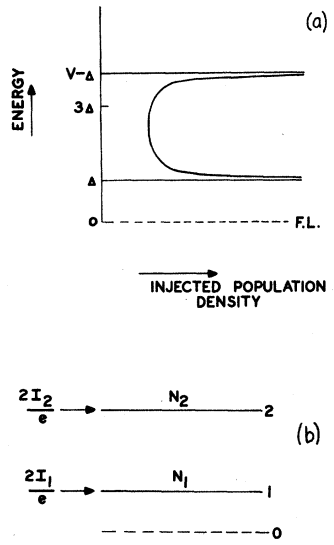

FIG. 4. (a) Distribution of the injected population vs energy. (b) Simplified equivalent three-level system.

tween 2 and 0. To take into account the excitations produced on both sides of the barrier we assume that $2I_1/e$ and $2I_2/e$ particles are injected per sec into levels 1 and 2, respectively, where e is the electronic charge. Let N_1 and N_2 be the instantaneous population in levels 1 and 2 and let τ' be the lifetime of an excitation in level 2. Following Rothwarf and Taylor[12] the detailed balance equations are as follows:

$$\frac{dN_2}{dt} = \frac{2I_2}{e} - \frac{N_2}{\tau'} + \alpha N_p N_1, \tag{8}$$

$$\frac{dN_1}{dt} = \frac{2I_1}{e} + \beta N_p - rN_1^2 + \frac{N_2}{\tau'} - \alpha N_p N_1, \tag{9}$$

$$\frac{dN_p}{dt} = \tfrac{1}{2} rN_1^2 - \tfrac{1}{2}\beta N_p + \frac{N_2}{\tau'} - \alpha N_p N_1 - \gamma (N_p - N_{p0}) + J, \tag{10}$$

where N_{p0} is the population of the phonon bath in thermal equilibrium and α, β, and r are constants defining the respective transition probabilities while γ is the rate of phonon escape to the constant temperature medium. J is the number of phonons absorbed by the detector per second from the incident phonon shower.

For the generator ($J=0$) in the steady state ($d/dt=0$) one may combine Eqs. (8)–(10) to obtain the obvious result

$$(I + 2I_2)/e = \gamma (M - M_0), \tag{11}$$

which states that the number of phonons escaping to the sapphire crystal is equal to $(I+2I_2)/e$, if we ignore those phonons that escape to the helium bath. Taking the generator as a point source emitting phonons in an isotropic medium the phonons absorbed by the detector per sec will be given by

$$J = \frac{a}{e}(I + 2I_2)\frac{A}{2\pi l^2}, \tag{12}$$

where a is a constant <1, and l is the length of the sapphire crystal. Using this value of J in (10) and combining Eqs. (8)–(10) the steady-state populations in the detector ($I_1 = I_2 = 0$) are given by

$$N_1^2 = N_{10}^2 + \frac{A}{2\pi l^2}\frac{\beta}{\gamma r}\frac{a}{e}(I + 2I_2) \tag{13}$$

for level 1 and

$$N_2 = \frac{\alpha \tau' \gamma}{\beta} N_1^3 \tag{14}$$

for level 2 where the thermal equilibrium values $\beta N_{p0} = rN_{10}^2$ were used.

We ignore the contribution of N_2 to the detector signal and put $n_e = N_1 - N_{10}$. Using the equilibrium populations per unit volume $n_{10} = N_{10}/Ad$ and $n_{p0} = N_{p0}/Ad$ one gets from (3) and (13)

$$\left(\frac{\delta}{2\Delta}\right)^{1/2} = \frac{n_{10}}{4\Delta N(0)} \times \left\{\left[1 + \left(\frac{a}{e}\right)(\gamma d \times 2\pi l^2 n_{p0})^{-1}(I + 2I_2)\right]^{1/2} - 1\right\}. \tag{15}$$

The detector signal is finally obtained by substituting (15) and (2) in (1). It is obvious that in general the signal at a fixed bias is not a linear function of the generator current I for $V < 4\Delta$. Furthermore, the dependence of the signal on temperature is determined not only by n_{10} and n_{p0} but also by its degree of excitation by the incident phonons. To estimate the order of magnitude of the different terms in (15) we calculate n_{10} and n_{p0}. Using the superconducting density of states and Fermi-Dirac distribution one obtains

$$n_{10} = 2\Delta N(0)\left(\frac{\pi t}{2b}\right)^{1/2} e^{-b/t}, \tag{16}$$

and from the Debye spectrum and Bose-Einstein distribution one gets

$$n_{p0} = 9N\left(\frac{bT_c}{\Theta}\right)^3 \frac{4t}{b} e^{-2b/t}, \tag{17}$$

which are valid for $\Theta/T \gg 2\Delta/kT \gg 1$. Here N is the number of atoms per unit volume, Θ is the Debye temperature, T_c is the superconducting transition temperature, $t = T/T_c$, and $b = \Delta_0/kT_c$. If we now linearize (15) and substitute n_{10} and n_{p0} from (16) and (17) one finds that the signal is a strong function of the temperature and will vary like $(b/t)^{1/2}e^{b/t}$. This temperature dependence diminishes with increasing excitation level and vanishes in the limit of high excitation. We calculate now the factor that determines the behavior of the signal for the following values of the parameters for Pb: $T = 1.2$ °K, $T_c = 7.19$ °K, $\Theta = 105$ °K, $N = 0.33\times10^{23}$ cm^{-3}, $N(0) = 1.824\times10^{22}$ eV^{-1}cm^{-3},[13] $l = 1$ cm, $a = 1$ and taking γd to equal 2×10^5 cm sec^{-1} ~the velocity of sound[12] in Pb one gets

$$(a/e)(\gamma d \times 2\pi l^2 n_{p0}) \sim 2.6\times10^3\ \text{A}^{-1}.$$

It is obvious that the acoustic mismatch between Pb and the sapphire substrate may reduce the value of a far below unity and that photon scattering at imperfections and dislocations in the sapphire may reduce the phonon shower density at the detector by an order of magnitude below that estimated here. However, the generator current is typically in the order of amps, and the detector response will not be linear in the current.

The integrals of Eqs. (6) and (7) can be obtained in terms of elliptic integrals. They can easily be put in a form appropriate for computation using subroutines available in the IBM scientific subroutine library. We compute the signal in the linear $S = C(I + 2I_2)$ and square root $S = C(I + 2I_2)^{1/2}$ limits, where C is a constant. The derivative $\partial S/\partial I$ is computed using Lagrangian interpolation polynomial

of degree 2 relevant to three successive points. The results shown in Figs. 5 and 6 are normalized such that both S and I equal one at $V = 6\Delta$, while the derivative is normalized by taking the constant $C = 1$. The solid and dashed curves depict the behavior in the linear and the square-root limits, respectively. The kink in the signal curve and the singularity in the derivative obviously occur at $I(4\Delta)$ and reflect the effect of the square-root singularity in the theoretical density of states of a superconductor at the gap.

One also finds that the ratio $S(6\Delta)/S(4\Delta)$ varies from 3.1 in the linear limit to 1.76 in the square-root limit. This ratio is an important parameter which links theory and experiment. One can write at constant bias

$$S(V) = C_1(\{1 + C_2[I(V) + 2I_2(V)]\}^{1/2} - 1) , \qquad (18)$$

where C_1 and C_2 are constants. Putting $x = C_2 I(6\Delta)$ and using for the currents the values $I_2(4\Delta) = 0$, $2I_2(6\Delta) = I(6\Delta)$, and $I(4\Delta) = 0.646 I(6\Delta)$ one obtains

$$S(6\Delta)/S(4\Delta) = [(1 + 2x)^{1/2} - 1]\,[(1 + 0.646x)^{1/2} - 1]^{-1}. \qquad (19)$$

The dependence of this ratio on x is depicted in Fig. 7. Since there is a good agreement between theoretical and experimental values of $I(V)$ one can use the experimental ratio $S(6\Delta)/S(4\Delta)$ in Fig. 7 to obtain the value of $C_2 I(6\Delta)$ appropriate to the experiment. Through proper normalization one can compare the theoretical prediction with the experimental results.

At a fixed generator current the detector signal vs bias can be written

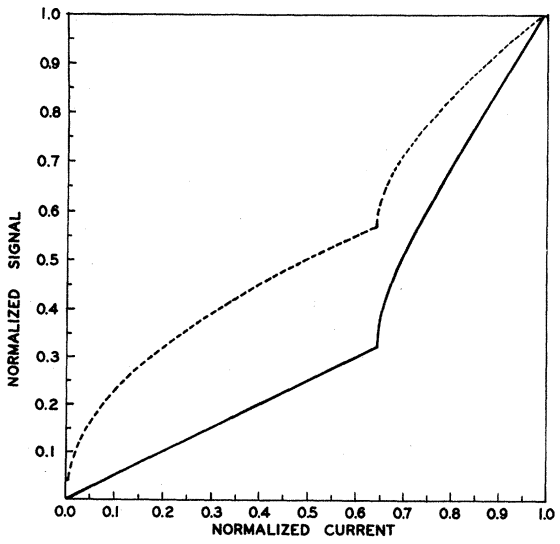

FIG. 5. Calculated signal vs current in the linear (solid) and square-root (dashed) limits, normalized such that $I(6\Delta) = 1$ and $S(6\Delta) = 1$ in both cases.

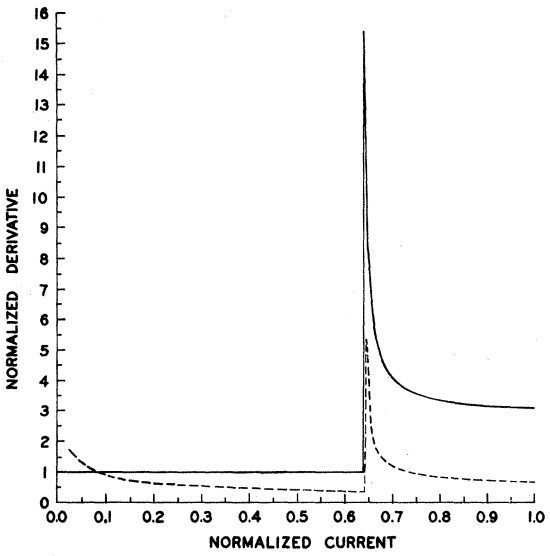

FIG. 6. Calculated derivatives of the signals shown in Fig. 5.

$$S(V_B) = C_3 \frac{R_d}{1 + R_B/R_L} \frac{V_B + \Delta}{[(V_B + \Delta)^2 - \Delta^2]^{1/2}} , \qquad (20)$$

and since it depends on one constant C_3, comparison with experiment is straightforward.

IV. EXPERIMENTAL RESULTS

A. Data Processing

As mentioned in the Introduction, all subsequent processing is carried out using the data sets equally spaced in the independent variable V or V_B. Various methods to smooth (filter) and differentiate the experimental data were attempted.[14] We found that the most suitable method is to calculate the least-square fit over an interval of 11 experimental points to a third-order expansion in terms of Chebyshev polynomials.[15] The expansion coefficients thus obtained yield immediately a smoothed value of the function at the point in the center of the interval as well as a good approximation to its derivative at that point. Although a higher degree of smoothing could be obtained by increasing the size of the interval, the correlation between the highly nonlinear experimental results and the polynomial expansion (even of higher order than the third) diminishes very rapidly and results in an extraneous fit to the experimental curve.

In comparing a theoretical prediction with an experimental curve the required scaling factors are calculated using similar techniques. We first calculate a smoothed value of the experimental function at a chosen point using the Chebyshev polynomial expansion. The smoothed value is then used to obtain the scaling factor.

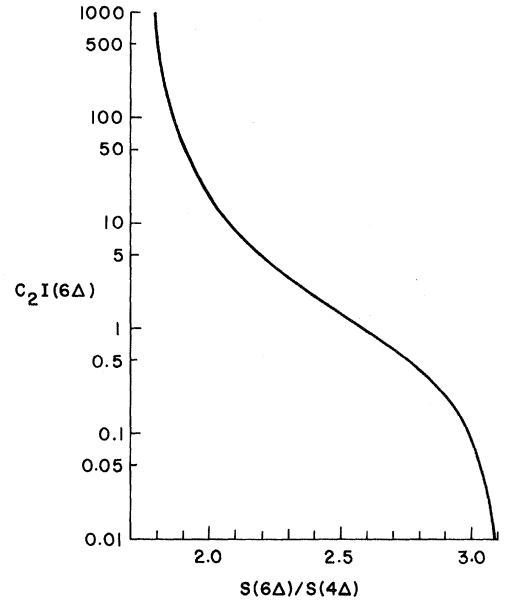

FIG. 7. Dependence of $C_2I(6\Delta)$ on the signal ratio $S(6\Delta/S(4\Delta)$.

B. Detector Signal vs Bias

The dependence of the detector signal on the bias is not only important but also quite intriguing and we proceed here to discuss it in some detail. From the various samples studied we present results for a particular diode where the Josephson constant voltage steps are confined to bias voltages below 0.5 mV. Its I_B-V_B characteristic in Fig. 8 clearly manifests the subharmonic structure described in Sec. II. Its response to the phonon shower is depicted by the solid lines in Figs. 9(a) and 9(b) for generator voltages $V = 2.24\Delta$ and 9Δ, respectively. Though the phonon spectra emitted at these generator voltages are expected to be quite distinct the detector response, except for a change in magnitude, remains essentially the same. This seems to lend some support to the assumption that the PBM furnishes the major contribution to the detected signal. We proceed therefore to compare the prediction of Eq. (20) with the experimental curve. With a scaling factor calculated at $V_B = 1.6$ mV, the behavior of the signal described by Eq. (20) is given by the dashed curves in Figs. 9(a) and 9(b).

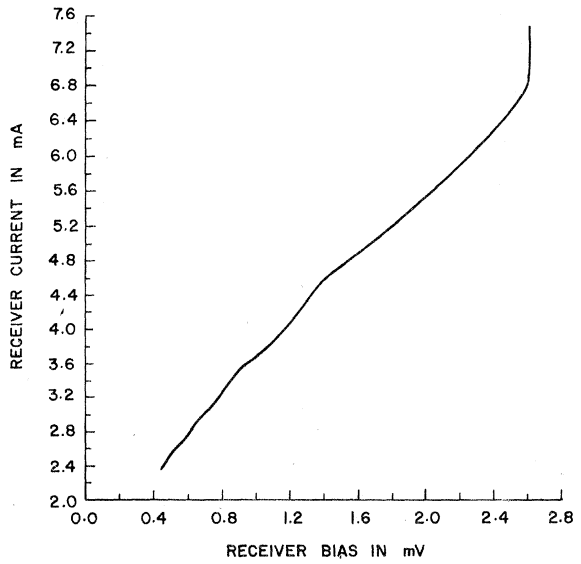

FIG. 8. I_B - V_B characteristic of the detector in an applied magnetic field of 30 G.

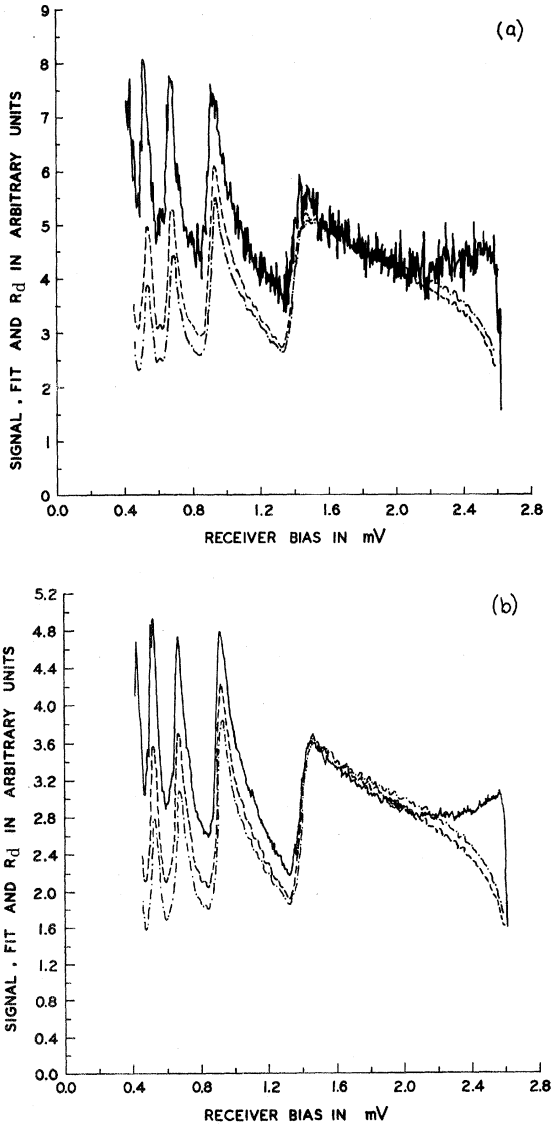

FIG. 9. Measured signal vs detector bias (solid), the theoretical fit due PBM (dash), and the dynamic resistance of the detector characteristic (dot dashed). Generator voltage (a) $V = 2.24\Delta$; (b) $V = 9\Delta$ ($\Delta = 1.32$ mV).

The dotted curves depict the dynamic resistance R_d scaled at the same point. All curves are quite similar in shape but the agreement is good only in the range $1.55 < V_B < 2.3$ mV. The deviation is by no means random and has a well-defined dependence on the bias voltage. This deviation cannot be attributed to the failure of the linear approximation $I_B(R_B - R_B') = iR_d$ [adopted in deriving Eq. (1)] because the maximum value of the signal in Fig. 9(b) is only ~4 μV.

Since Eq. (1) remains valid no matter which mechanism is responsible for the signal current i we should invert Eq. (1) and plot

$$i(V_B) = C_4 |S| (1 + R_B/R_L)/R_d .$$

In this way we get rid of the effect of the nonlinearities in the I_B-V_B characteristic and obtain the actual signal current induced by the phonon shower. Scaling again at $V_B = 1.6$ mV one gets the astonishing results depicted in Figs. 10(a) and 10(b). The signal current is nonanalytic, possesses singularities at $V_B = 0$ and $V_B = 2\Delta$ and has finite jumps approximately at the subharmonic voltages $V_B = 2\Delta/n$.[16] The singularity at $V_B = 0$ can be taken care of by the current given by Eq. (2) owing to the PBM. To explain the sharp rise near $V_B = 2\Delta$, one has to invoke the presence of a measurable contribution coming from PAT. Before going into more detailed discussion let us first introduce two more curves [Figs. 11(a) and 11(b)] which show the dependence on V_B of the ratio of the measured signal to that calculated from Eq. (20) scaled at the same bias $V_B = 1.6$ mV. These curves essentially represent the "excess" signal over that expected from PBM. The sharp rise near $V_B = 2\Delta$ remains practically unchanged since, as evident from (20), the PBM contribution diminishes only slightly in this region. The striking difference, however, especially evident in Fig. 11(b) is that the excess signal between the jumps at the subharmonic voltages is now constant. Incrementing the normalization factor by some 13% at each step would therefore result in full agreement between the measured signal and that calculated from PBM for $V_B < 2$ mV. In Fig. 11(a) these steps though constant over most of their range, deviate by an amount ~ the noise amplitude at the right end. However, calculation at other generator voltages yielded constant steps similar to those in Fig. 11(b) but with different increments in the required normalization factor. The required increments are ~ 20, 17, 15, 13, and 12% at $V/\Delta = 2.24$, 5, 7, 9, and 11, respectively.

In PAT[11] a phonon of energy ω will increment the signal current at $2\Delta - \omega \leq V_B \leq 2\Delta$ by an amount identical in shape to the diode I-V characteristic at $2\Delta \leq V \leq 2\Delta + \omega$. Given the phonon spectrum in the incident shower one could use Kleinman's analysis[11] to calculate the contributions from PAT. Assuming a constant matrix element for PAT and a uniform phonon distribution we calculated a current $i(V_B)$ and added it with an adjustable parameter to (20). The fit to experimental results was consistently worse than that we already have using (20) alone. If the matrix element for PAT is indeed constant independent of the phonon energy the experimental result suggests the existence of a large peak at the low-energy end of the phonon spectrum similar to that calculated by Kinder *et al.*[6] It is evident, however, that our understanding is still quite poor and more detailed analysis and measurement are required.

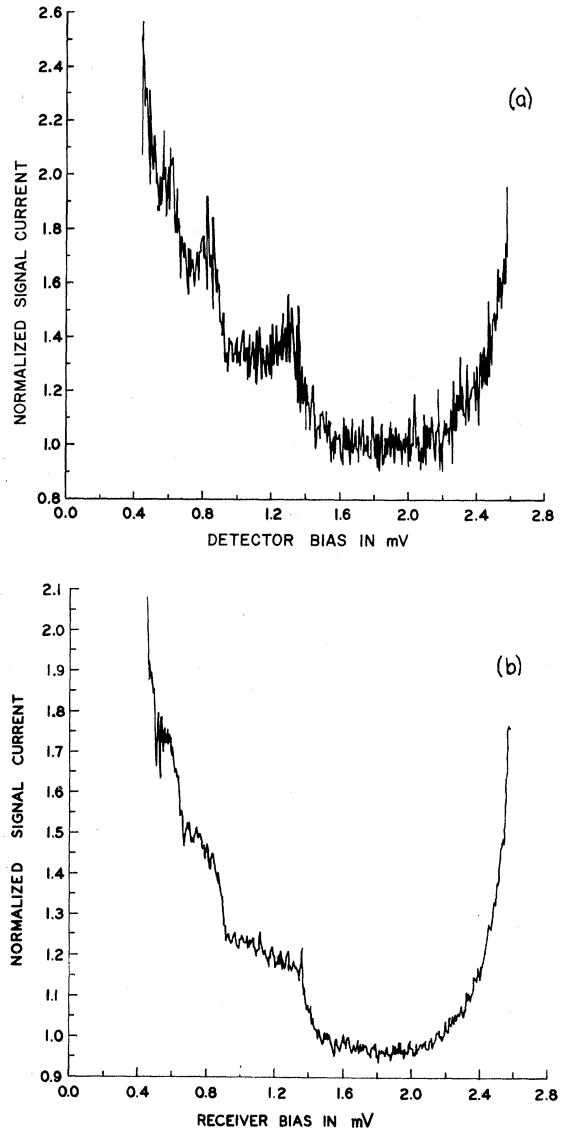

FIG. 10. Normalized signal current vs detector bias. (a) $V = 2.24\Delta$; (b) $V = 9\Delta$.

C. Detector Signal vs Generator Current

The detector signal vs generator current is

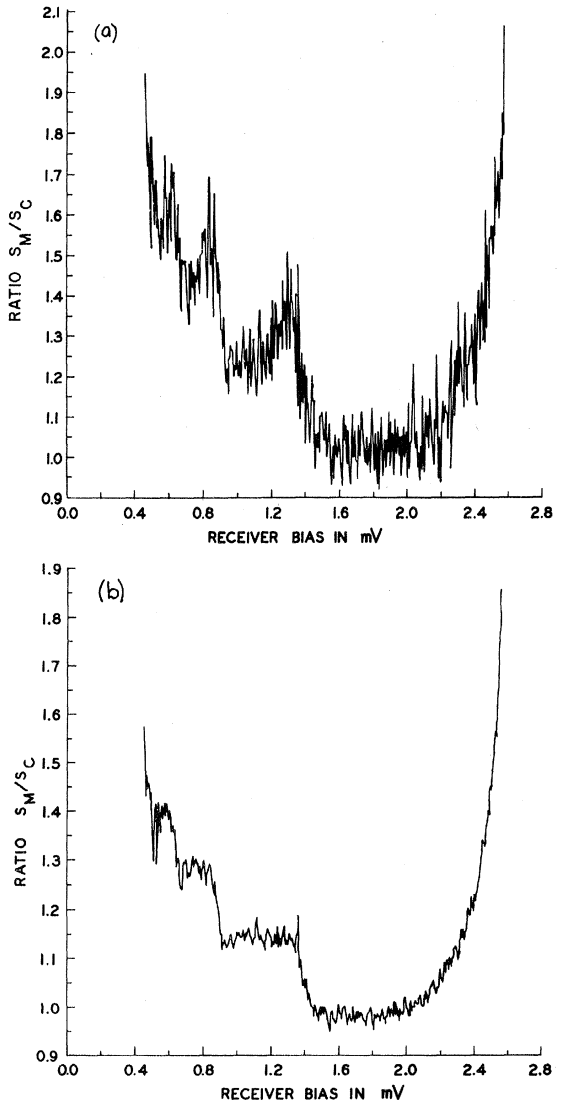

FIG. 11. Ratio of measured signal to that calculated from PBM vs detector bias: (a) $V=2.24\Delta$; (b) $V=9\Delta$.

shown in Fig. 12 together with the V-I characteristic of the generator. The general qualitative agreement with Fig. 5 is obvious and the signal behavior corresponds to an intermediate case between the linear and square-root limits. The ratio $S(6\Delta)/S(4\Delta)$ is ~ 2 and yields from Fig. 7 the value of $C_2 I(6\Delta) \sim 18$. No attempt was made, however, to compute a fit to the measured signal using Eq. (18). The details of the signal for larger currents show more clearly in $\partial S/\partial I$ which is discussed in Sec. IV D.

D. Signal Derivatives vs Generator Voltage

In this section we present $\partial V/\partial I$ and $\partial S/\partial I$ and their respective derivatives with respect to V using the smoothing and differentiation method described in Sec. IV A. The smoothed first derivatives are

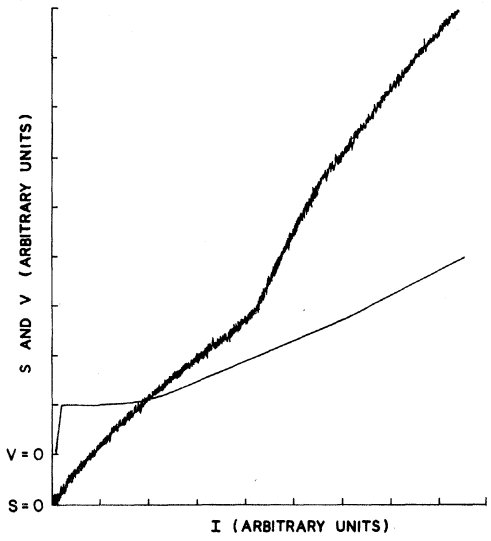

FIG. 12. Measured signal S at fixed bias and generator voltage V vs generator current I.

shown by the solid curve and the original experimental data by the dots. The differential resistance D of the generator is shown in Fig. 13 where the experimental data are sufficiently smooth that all the dots lie on the solid curve. The second derivative $\partial D/\partial V$ is shown in Fig. 14 together with the Pb phonon spectrum $[\alpha^2(\omega)F(\omega)]$ with its origin shifted to the right by an amount $= 2\Delta$. This spectrum was plotted using numerical tables of $\alpha^2 F$ for lead kindly given to us by Rowell and McMillan.[18] The vertical solid lines show the positions of the Van Hove critical points obtained from Table I of Ref. 17. There is an excellent agreement between

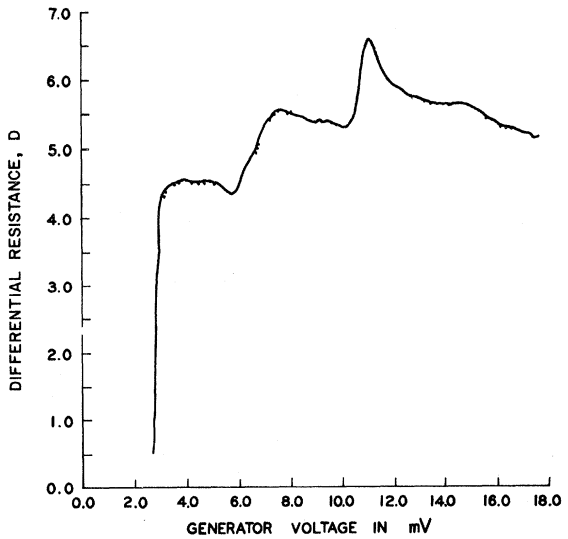

FIG. 13. Smoothed differential resistance D (solid) of the generator with the original experimental values (dots) everywhere coincident with the solid curve.

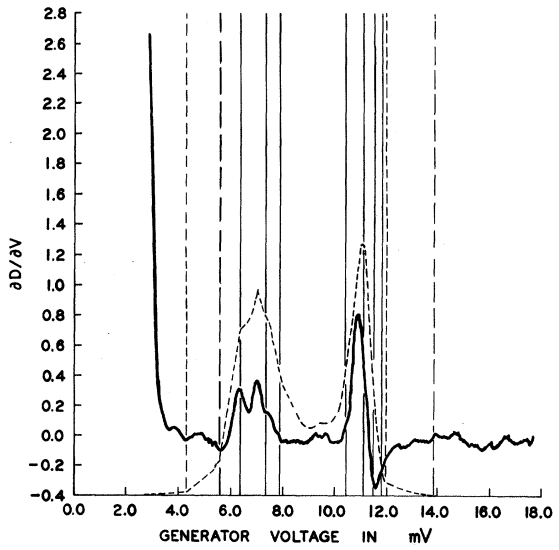

FIG. 14. Calculated $\partial D/\partial V$(solid) together with $(\alpha^2 F)$ for Pb (dashed) from Ref. 18. The solid vertical lines show the position of the Van Hove critical points obtained from Ref. 17 and the dashed lines other critical points of the spectrum.

our results and those obtained by Rowell and Kopf (Fig. 8, Ref. 17) showing that the methods we use here are of comparable accuracy.

We turn now to the signal derivative $D' = \partial S/\partial I$ shown in Fig. 15 together with the spectrum. One immediately sees that here, as in the generator, all the details of spectrum are reflected in D'. This leads to the tentative conclusion that at a large enough voltage the phonon spectrum emitted from a Pb-Pb tunnel diode will closely resemble the phonon spectrum of Pb. Naturally, one will find a large peak of finite width in the phonon population at $\omega \sim 2\Delta$ coming from recombination. The width of this peak will determine the population at the low-energy end of the emitted spectrum, the narrower the peak the larger this population. Obviously, this will happen if we assume that the majority of the generated phonons can escape to the substrate without any further interaction. We pursue this assumption in some detail in the following paragraph.

There is good qualitative agreement for $V < 6\Delta$ between the measured derivative and that calculated from the simple model shown in Fig. 6. Quantitatively, however, the agreement is poor because of the large effect of the electron-phonon interaction due to the presence of the transverse-phonon peak ω_t in this region. It is difficult to explain the existence in D' of structure so closely related to that of the transverse-phonon peak. The difficulty here comes from the fact that two large contributions to D' are occurring simultaneously: (a) The emitted phonon spectrum is rapidly varying as the singularity of the electron density of states sweeps across the phonon peak at ω_t, and (b) the onset of the detector response to the relaxation phonons is manifesting itself by the jump in D' at $V = 4\Delta$ and the subsequent rapid drop as calculated from the simplified three-level model. Near the longitudinal peak ω_l the situation is probably simpler and lends itself to the following interpretation. As $(V - 2\Delta)$ approaches ω_l the population of the longitudinal phonons starts to build up and will continue to do so [even for $(V - 2\Delta) > \omega_l$] as more and more excitations can couple to a larger number of phonon modes belonging to the longitudinal peak. For some $(V - 2\Delta) > \omega_l$ this population will reach a maximum as evident in Fig. 15. Competing processes will tend to transfer the excitation energy to the lower-frequency part of the spectrum. However, the magnitude and correct shape and position of the peak in D' relative to ω_l leads to the conclusion that the emitted phonon spectrum contains a considerable population in the longitudinal peak for $(V - 2\Delta) > \omega_l$. Similar arguments will lead to similar conclusions near ω_t. Finally we present $\partial D'/\partial V$ in Fig. 16 obtained as described in Sec. IV A. The resolution is poor because of the large noise in D' as evident from the scatter of the points relative to the solid curve in Fig. 15. All one could claim is the presence of a wide hump indicated by the dot-dashed line in Fig. 16 which occurs in the same voltage range covered by the phonon spectrum. Thus, in the extreme case where the majority of the generated phonons can escape to the substrate with no further interaction, an adequate interpretation of the structure in D' is obtained. We discuss now the other extreme where all excitations rapidly

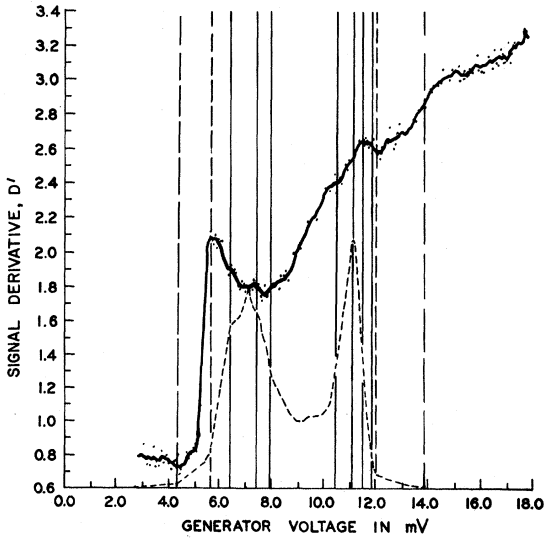

FIG. 15. Smoothed derivative D' of the signal (solid) and the original experimental data (dots) together with $\alpha^2 F$ (dashed) and the critical points as in Fig. 14.

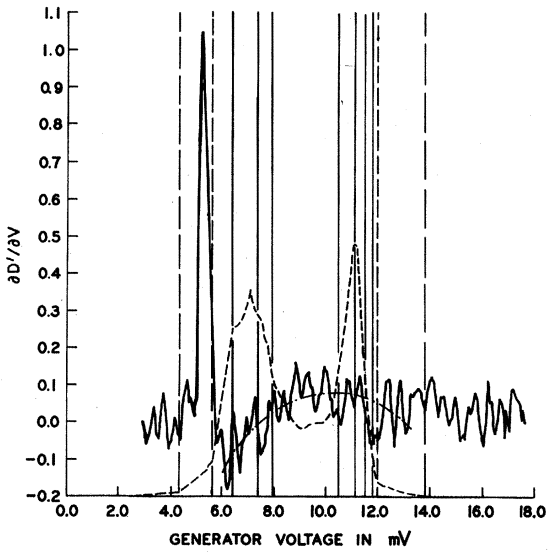

FIG. 16. Calculated $\partial D'/\partial V$ (solid) together with α^2F (dashed) and the critical points as in Fig. 14.

thermalize by comparing the tunnel diode with an ordinary heater.

In a heater one uses a highly disordered alloy so that sufficient energy can be delivered to the phonon gas due to I^2R losses at moderately small currents. In such an alloy the electron mean free path is small and the energy gained by an electron accelerated by the applied field is also small. Thus on the average all the excitations produced in the electron gas lie close to the Fermi level and hence on decaying will emit low-frequency phonons. Although the heater is not in thermal equilibrium, Narayanamurti[19] has shown that the resulting phonon spectrum can adequately be represented by a Planck's distribution from a blackbody radiator at some characteristic temperature greater than the ambient temperature. To raise the characteristic temperature one applies a larger electric field forcing the electrons to gain more energy between collisions and hence shifting the peak in the generated phonons towards higher energy. In contrast the tunnel diode offers a simple device in which high-energy excitations can be produced as shown in Fig. 3(a). The initial decay of an energetic quasiparticle may result in the emission of a high-energy phonon which has a finite probability of escaping into the substrate. These phonons have an energy distribution resembling the phonon spectrum of the metal modified by the distribution of the injected quasiparticles and the relative life times. But the lifetime of a high-energy excitation, particle, or phonon, is extremely small and it is doubtful that in the steady state there exist populations of particles or phonons large enough to account for the structure observed in the signal derivative D'. The smallness of these lifetimes implies that all excitation energy is rapidly converted to the low-frequency phonons as well as to the recombination phonons of energy 2Δ. If such rapid thermalization takes place the structure in D' is simply explained as follows. Increasing the generator current and voltage from I and V to $(I+\delta I)$ and $(V+\delta V)$ will increase the input power by $(I\delta V + V\delta I)$. If δI is constant, the power increment is proportional to $V(1+D/R)$ and with rapid thermalization the increment in the 2Δ phonons will be proportional to the same quantity. Hence D' is approximately a linear function of the generator voltage and contains all the structure appearing in D. This behavior is quite similar to that of D' in Fig. 15 for $V > 6\Delta$.

V. SUMMARY

Phonons incident on the detector produce an increase in the tunneling current by an amount $i(V_B)$ which is shown in Figs. 10(a) and 10(b) at generator voltages $V = 2.24\Delta$ and 9Δ, respectively. This increase in the tunneling current can be due to (a) the enhancement by the incident phonons of the steady-state population of the excited quasiparticles, and (b) the existence of additional tunneling channels in the presence of the incident phonons. The general behavior of $i(V_B)$ is summarized as follows.

(i) The shape of $i(V_B)$ shows little dependence on the generator voltage, and hence on the emitted phonon spectrum.

(ii) The enhancement of the excited quasiparticle population by incident phonons of energy $\geq 2\Delta$ does not fully account for the measured $i(V_B)$.

(iii) The large increase in $i(V_B)$ as $V_B \to 2\Delta$ can be attributed to phonon-assisted tunneling if the emitted phonon spectrum has a large population of low-energy phonons.

(iv) If one views the jumps in $i(V_B)$ at $V_B \sim 2\Delta/n$ to be due to additional tunneling channels, one concludes that all channels are open at $V_B = 0$ and sequentially close as V_B is increased to coincide with one subharmonic values (starting with the largest value of n).

From the dependence of the detector signal S and its derivative D' on the generator voltage (see Figs. 12 and 15) one may draw the following conclusions.

(a) At $V = 4\Delta$ there is a well-defined kink in S, and hence a jump in D', which occur when the relaxation of injected excitations to the top of the gap starts to yield phonons of $\omega = 2\Delta$. From this we conclude that the major contribution to S comes from those phonons of $\omega \geq 2\Delta$ which in breaking Cooper pairs in the detector result in an enhancement of the steady-state population of excited quasiparticles.

(b) The deviation from linearity in the dependence of S on I for $V < 4\Delta$ clearly indicates the increase in the recombination rate of quasiparticle excitations in the detector as their steady-state population in-

creases with increasing phonon density in the incident shower.

(c) The drop in D' following the jump at $V = 4\Delta$ results from the effect of the singularity in the electron density of states at the gap edge on the increment in the number of relaxation phonons of $\omega \geq 2\Delta$ (compare with model calculation shown in Fig. 6).

(d) In addition to these three major features, we were able to resolve in D' structure closely related to α^2F for Pb as shown in Fig. 15. Using rather vague arguments we were able to infer that this structure should appear in D' in either of the two extreme cases.

(1) All phonons resulting from the first decay of the injected excitations escape the film with no further interaction. In this case, the structure in D' shows the dominance of the electron-phonon interaction (e.g., at $\omega \sim \omega_i$) over the electron-electron interaction since the latter will tend to transfer the high excitation energies to lower-frequency phonons.

(2) All high-energy excitations, particles, and phonons rapidly thermalize. In this case, the resulting increment in the recombination phonons of $\omega \sim 2\Delta$ will be proportional to the power increment $(I\delta V + V\delta I)$ and hence D' will contain structure similar to that in D.

More detailed analysis is required to determine the emitted phonon spectrum. In general, however, the spectrum is expected to have the following properties.

(a) There is a sharp peak in population at $\omega \sim 2\Delta$ due to recombination.

(b) The relaxation should yield a phonon distribution which can be represented by $f(E, V)F(\omega)h(\omega)$ where f is the injected particle density at $E = \omega + \Delta$, F is the phonon density of states, and h is an energy-dependent reduction factor which depends on the mean free path of a given excitation relative to the film thickness. In the limit of rapid thermalization the function $h(\omega)$ will tend to the Bose-Einstein distribution $(1 + e^{\omega/kT_e})^{-1}$ where T_e is some effective temperature of the generator.

ACKNOWLEDGMENTS

We would like to thank W. L. McMillan and J. M. Rowell for many useful discussions and comments on the manuscript.

[1]W. Eisenmenger and A. H. Dayem, Phys. Rev. Letters 18, 125 (1967).

[2]L. Tewordt, Phys. Rev. 127, 371 (1962).

[3]V. L. Pokrovskii, Zh. Eksperim. i Teor. Fiz. 40, 898 (1961)[Sov. Phys. JETP 13, 628 (1961)].

[4]W. L. McMillan and J. M. Rowell, in *Superconductivity*, edited by R. D. Parks (Marcel Dekker, New York, 1969).

[5]A. Rothwarf, Phys. Rev. Letters 23, 468 (1969).

[6]H. Kinder, K. Laszmann, and W. Eisenmenger, Phys. Letters 31A, 475 (1970).

[7]D. J. Scalapino, in Ref. 4.

[8]B. N. Taylor and E. Burstein, Phys. Rev. Letters 10, 14 (1963); J. R. Schrieffer and J. W. Wilkins, *ibid.* 10, 17 (1963); J. M. Rowell and W. L. Feldmann, Phys. Rev. 172, 393 (1968); I. Giaever and H. R. Zeller, Phys. Rev. B 1, 4278 (1970).

[9]The magnitude of this leakage current depends critically on the degree of smoothness of the sapphire substrate. Due to the hardness of the sapphire it is practically impossible to obtain a surface free of pits and scratches. Using quartz single crystals which can be polished to a high degree of smoothness we were able to make diodes where the leakage current was $< 10^{-3}$. However, the imperfections and high dislocation density in the quartz resulted in a reduction of the signal by about one order of magnitude in the best quartz crystals we used.

[10]R. E. Eck, D. J. Scalapino, and B. N. Taylor, Phys. Rev. Letters 13, 15 (1964); D. D. Coon and M. D. Fiske, Phys. Rev. 138, A744 (1965).

[11]L. Kleinman, Phys. Rev. 132, 2484 (1963).

[12]A. Rothwarf and B. N. Taylor, Phys. Rev. Letters 19, 27 (1967).

[13]W. L. McMillan, Phys. Rev. 167, 331 (1968).

[14]We used the various smoothing subroutines available in the IBM System/360 scientific subroutine library.

[15]This fit was obtained using subroutines APCH and APFS from Ref. 14. There, the rapid convergence of a Chelyshev polynomial expansion in comparison to a power-series expansion is discussed and pertinent references are listed.

[16]We use the expression "subharmonic" structure at $V_B = 2\Delta/n'$ rather loosely, since, as found by Rowell and Feldmann (Ref. 7), there is no unique value of Δ which determines the actual position of this structure.

[17]J. M. Rowell and L. Kopf, Phys. Rev. 137, A907 (1965).

[18]J. M. Rowell and W. L. McMillan (unpublished). Numerical tables of α^2F, real and imaginary parts of the gap, and the renormalization function determined from tunneling data for various superconducting metals and alloys.

[19]V. Narayanamurti, Phys. Letters 30A, 521 (1969).